Journal of Ceramic Processing Research. Vol. 17, No. 8, pp. 789~794 (2016)

J O U R N A L O F
Ceramic Processing Research

Enhanced mechanical properties of nanostructured (W,Ti)C-FeAl hard materials rapidly sintered by the pulsed current activated heating

In-Jin Shon*

Division of Advanced Materials Engineering, the Research Center of Hydrogen Fuel Cell, Chonbuk National University, 664-14 Deokjin-dong 1-ga, Deokjin-gu, Jeonju, Jeonbuk 561-756, Korea

In the case of cemented (W,Ti)C, Co or Ni is added as a binder for the formation of composite structures. However, the high cost of Co or Ni, the low hardness and the low corrosion resistance of the (W,Ti)C-Ni and (W,Ti)C-Co cermets have generated interest in recent years for alternative binder phases. In this study, FeAl was used as a novel binder and consolidated by the pulsed current activated sintering (PCAS) method. The advantage of this process is not only rapid densification to near theoretical density but also the prohibition of grain growth in nano-structured materials. Highly dense (W,Ti)C-FeAl with a relative density of up to 99% was obtained within 3 minutes by PCAS under a pressure of 80 MPa. The addition of FeAl to (W,Ti)C enhanced the toughness without great decrease of hardness due to crack deflection and decrease of grain size.

Key words: Carbides, Nanostructures, Mechanical properties, X-ray diffraction, Sintering.

Introduction

(W,Ti)C has a high melting point and high hardness. In this regard, the transition metal carbide is primarily used as cutting tools and abrasive materials as a single phase or composite structures. In the case of cemented (W,Ti)C, Co or Ni is added as a binder for the formation of composite structures. However, the high cost of Co or Ni and the low corrosion resistance of the (W,Ti)C-Co or (W,Ti)C-Ni cermet have generated interest in recent years to find alternative binder phases [1-4]. It has been reported that iron aluminides show a higher oxidation resistance, a higher hardness and a cheaper materials compared to Co and Ni [5].

The improvement of mechanical properties and stability of cemented carbides could be also achieved by microstructural changes such as grain size refinement [6, 7]. Recently, nanocrystalline powders have been produced by high-energy milling [8, 9]. The sintering temperature of high-energy mechanically milled powder is lower than that of unmilled powder due to the increased reactivity, internal and surface energies, and surface area of the milled powder, which contribute to its so-called mechanical activation [10-12]. However, the use of conventional methods to consolidate nanopowders often leads to grain growth due to the extended time for sintering. Generally, the grain growth could be minimized by sintering at lower temperatures and for shorter times. In this regard, the pulsed current activated sintering (PCAS) technique has been shown to be effective in the sintering of nanostructured materials in a very short time [13-16].

We present here the results of the sintering of (W,Ti)C and (W,Ti)C-FeAl composites by pulsed current activated sintering with simultaneous application of pulsed current and high-pressure. The goal of this study was to produce dense and nanocrystalline (W,Ti)C and (W,Ti)C-FeAl hard materials in very short sintering times (< 3 min). The effect of novel FeAl binder on the mechanical properties, consolidation, and microstructure of (W,Ti)C-FeAl composites was also examined.

Experimental Procedures

The (W,Ti)C powder with a grain size of <1 mm and 99% purity used in this research was supplied by H.C. Starck. FeAl (<45 μm, 99.5% pure, Sejong Co.) was used as binder material. Three various compositions of (W,Ti)C, (W,Ti)C-5 vol.%FeAl, and (W,Ti)C-10 vol.%FeAl have been investigated. The powder was first milled in a high-energy ball mill (Pulverisette-5 planetary mill) at 250 rpm for 10 h. Tungsten carbide balls (9 mm in diameter) were used in a sealed cylindrical stainless steel vial under an argon atmosphere. The weight ratio of balls-to-powder was 30 : 1. Milling resulted in a significant reduction in grain size. The grain size of the (W,Ti)C was calculated from the full width at half-maximum (FWHM) of the diffraction peak by Suryanarayana and Grant Norton's formula [17].

$$B_r(B_{crystalline} + B_{strain}) \cos\theta = k\,\lambda / L + \eta\sin\theta \quad (1)$$

where B_r is the full width at half-maximum (FWHM)

*Corresponding author:
Tel : +82-63-270-2381
Fax: +82-63-270-2386
E-mail: ijshon@chonbuk.ac.kr

of the diffraction peak after instrument correction; $B_{crystalline}$ and B_{strain} are FWHM caused by small grain size and internal stress, respectively; k is constant (with a value of 0.9); λ is wavelength of the X-ray radiation; L and θ are grain size and internal strain, respectively; and θ is the Bragg angle. The parameters B and B_r follow Cauchy's form with the relationship: $B = B_r + B_s$, where B and B_s are the FWHM of the broadened Bragg peaks and the standard sample's Bragg peaks, respectively.

The milled powders were placed in a graphite die (outside diameter, 35 mm; inside diameter, 10 mm; height, 40 mm) and then introduced into the pulsed current activated sintering (PCAS) system made by Eltek Co. in the Republic of Korea. A schematic diagram of this system is shown in Ref. [18-20]. The PCAS apparatus includes a 30 kW power supply and a uniaxial press with a maximum load of 50 kN. The system was first evascuated and a uniaxial pressure of 80 MPa was applied. A pulsed current (on time; 20 μs, off time; 10 μs) was then activated and maintained until the densification rate became negligible, as indicated by the observed shrinkage of the sample. Sample shrinkage was measured in real time by a linear gauge measuring the vertical displacement. Temperature was measured by a pyrometer focused on the surface of the graphite die. A temperature gradient from the surface to the center of the sample is dependent on the heating rate, the electrical and thermal conductivities of the compact, and its relative density. The heating rates were approximately 800 K minute^{-1} during the process. At the end of the process, the current was turned off and the sample was allowed to cool to room temperature. The entire process of densification using the PCAS technique consists of four major control stages: chamber evacuation, pressure application, power application, and cooling off. The process was carried out under a vacuum of 11 Pa.

The relative densities of the sintered samples were measured by the Archimedes method. Microstructural information was obtained from the product samples, which had been polished and etched, using Murakami's reagent (10 g potassium ferricyanide, 10 g sodium hydroxide, and 100 ml water), for 1-2 minutes at room temperature. Compositional and microstructural analyses of the products were carried out through X-ray diffraction (XRD), scanning electron microscopy (SEM) with energy dispersive X-ray spectroscopy (EDS) and field-emission scanning electron microscopy (FE-SEM). Vickers hardness was measured by performing indentations at a load of 20 kg_f with a dwell time of 15 s.

Results and Discussion

Fig. 1 shows FE-SEM images of (W,Ti)C, (W,Ti)C-5 vol.%FeAl, and (W,Ti)C-10 vol.%FeAl powder milled for 10 h. The powders have a round grain shape and become more refined with milling time. Particle size of (W,Ti)C was calculated from the plot of B_r ($B_{crystalline} + B_{strain}$) cosθ versus sinθ in Suryanarayana and Grant Norton's formula [17]. The average grain sizes of the WC in the WC, WC-5 vol.%FeAl, and WC-10 vol.%FeAl powders after milling for 10 h calculated from the XRD data were about 20, 17 and 16 nm, respectively.

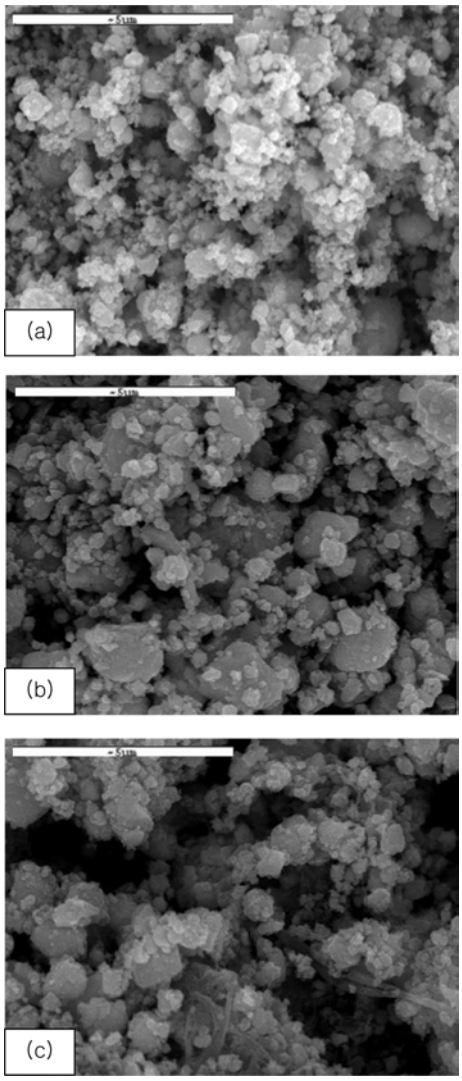

Fig. 1. FE-SEM images of powders milled for 10 h : (a) (W,Ti)C, (b) (W,Ti)C-5 vol.%FeAl, and (c) (W,Ti)C-10 vol.%FeAl.

The variations of shrinkage and temperature with heating time during the sintering of (W,Ti)C, (W,Ti)C-5 vol.%FeAl, and (W,Ti)C-10 vol.%FeAl powder by PCAS under 80 MPa pressure and pulsed DC current of 2800 A are shown in Fig. 2. In all cases, the application of the pulsed current resulted in shrinkage due to consolidation. The temperature of shrinkage initiation and abrupt shrinkage was reduced remarkably by the addition of FeAl. So, it is expected that FeAl would be molten during the sintering process. The main densification mechanism for this is the rearrangement of carbide particles, enhancement of the diffusion, and viscous flow of the binder [21].

Fig. 3 shows the XRD patterns of (W,Ti)C, (W,Ti)C-

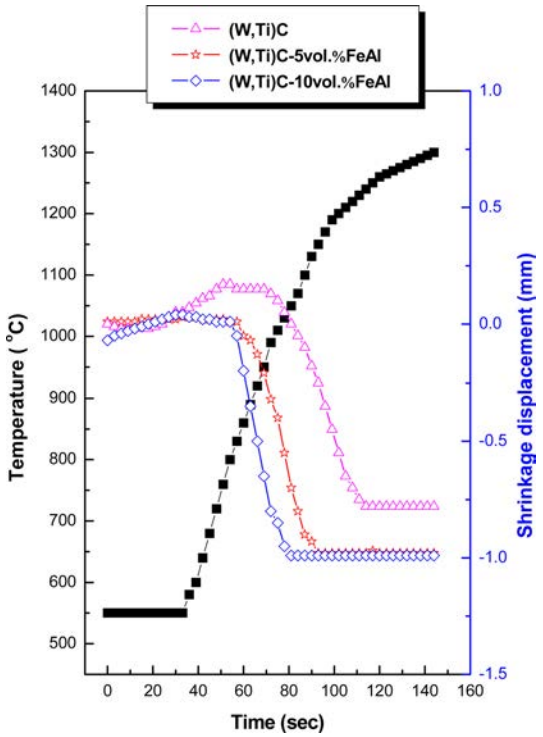

Fig. 2. Variation of temperature and shrinkage with heating time during the sintering of (W,Ti)C, (W,Ti)C-5 vol.%FeAl, and (W,Ti)C-10 vol.%FeAl.

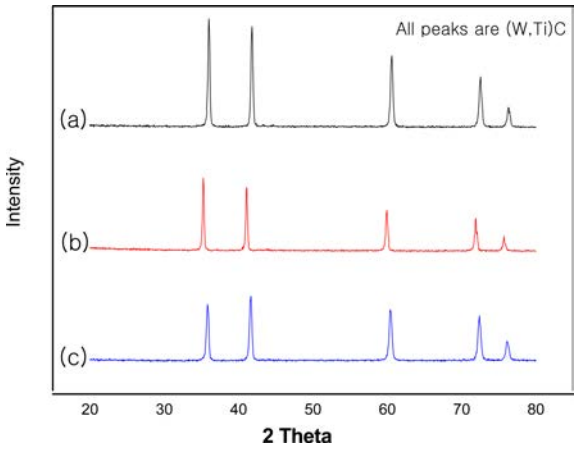

Fig. 3. XRD patterns of (a) (W,Ti)C, (b) (W,Ti)C-5 vol.%FeAl, and (c) (W,Ti)C-10 vol.%FeAl sintered by PCAS.

5 vol.%FeAl, and (W,Ti)C-10 vol.%FeAl after sintered by the PCAS method. In all cases, only (W,Ti)C peaks are detected and heavier contaminants, such as iron from a milling container, were not detected.

Plot of B_r ($B_{crystalline} + B_{strain}$) cosθ versus sinè in Suryanarayana and Grant Norton's formula is shown in Fig. 4. The average grain sizes of the (W,Ti)C calculated from the XRD data are about 60, 62, and 71 nm for the samples with (W,Ti)C, (W,Ti)C-5 vol.%FeAl, and (W,Ti)C-10 vol.%FeAl. FE-SEM images of the etched samples after being sintered up to about 1300 °C are shown in Fig. 5. From the figure, it is apparent that the grain size of (W,Ti)C consists of nanocrystallites. Thus, the

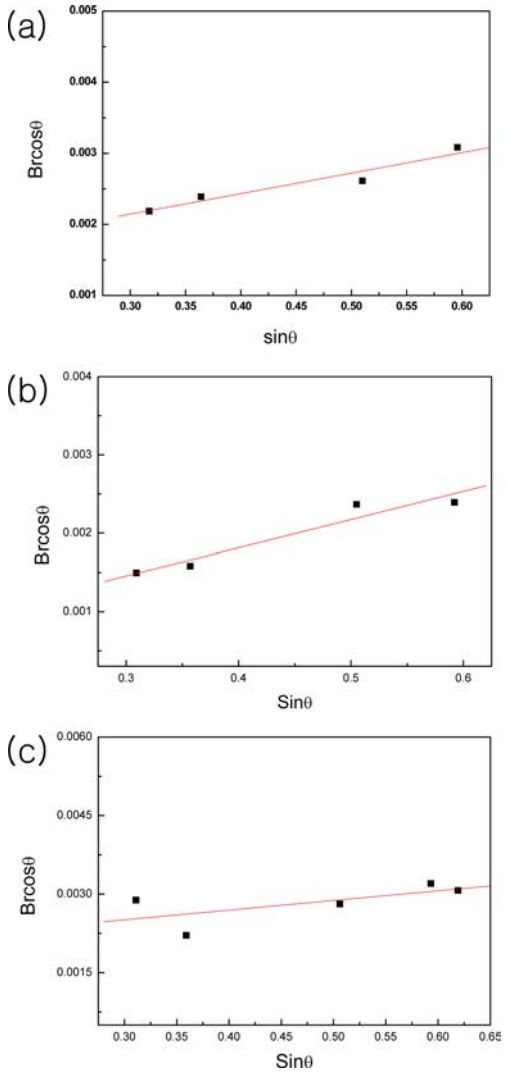

Fig. 4. Plot of B_r cosθ versus sinθ for (W,Ti)C in (a) (W,Ti)C, (b) (W,Ti)C-5 vol.%FeAl, and (c) (W,Ti)C-10 vol.%FeAl hard materials produced by PCAS.

average grain size of the sintered (W,Ti)C is not much larger than that of the initial powder, indicating the absence of grain growth during sintering. This retention of the grain size is attributed to the high heating rate and the relatively short term exposure of the powders to the high temperature. Relative densities corresponding to (W,Ti)C, (W,Ti)C-5vol.%FeAl, and (W,Ti)C-10 vol.%FeAl were approximately 99%.

The role of the pulsed current in sintering has been the focus of several attempts to provide an explanation for the observed sintering enhancement and the improved characteristics of the products. The role played by the pulsed current has been variously interpreted. The effect has been explained by fast heating due to Joule heating at contacts points, the presence of plasma in pores separating powder particles, and the intrinsic contribution of the current to fast mass transport [22-25].

Vickers hardness measurements were performed on polished sections of the (W,Ti)C, (W,Ti)C-5 vol.%FeAl,

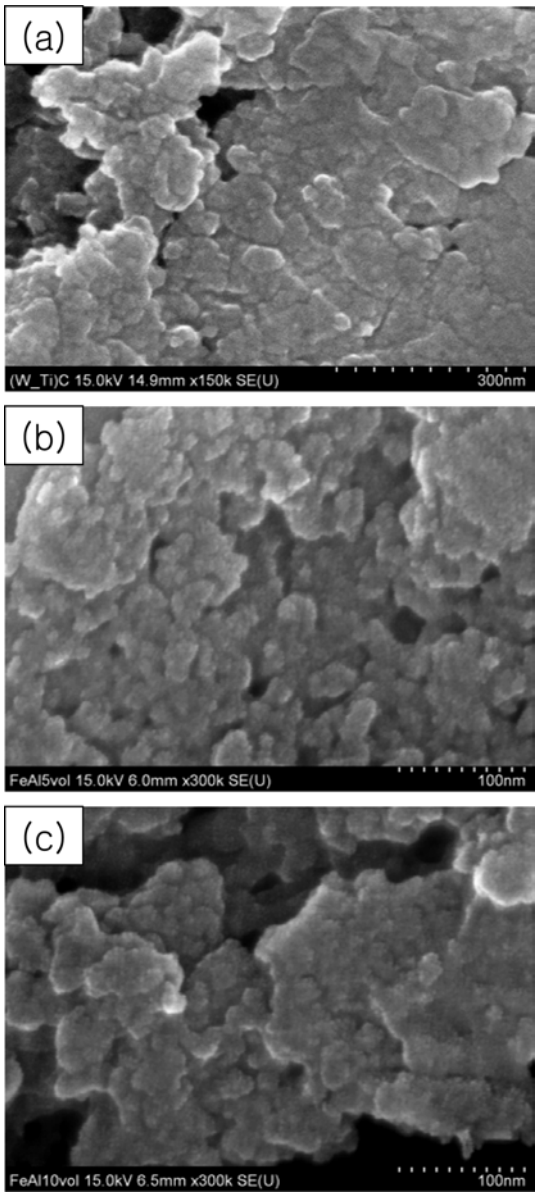

Fig. 5. FE-SEM images of (a) (W,Ti)C, (b) (W,Ti)C-5 vol.%FeAl, and (c) (W,Ti)C-10 vol.%FeAl hard materials produced by PCAS.

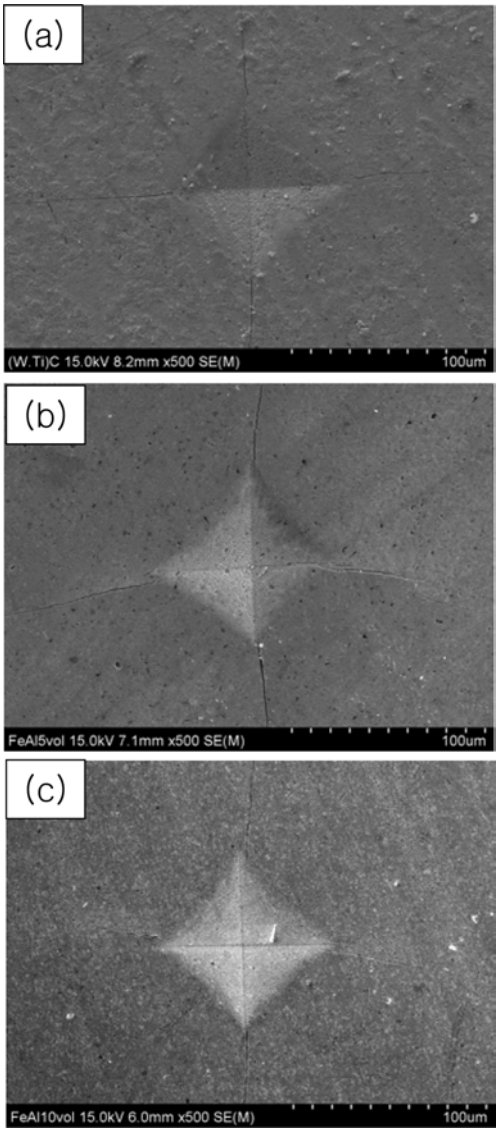

Fig. 6. Vickers hardness indentation in (a) (W,Ti)C, (b) (W,Ti)C-5 vol.%FeAl, and (c) (W,Ti)C-10 vol.%FeAl hard materials produced by PCAS.

and (W,Ti)C-10 vol.%FeAl samples using a 20 kg_f load and 15 s dwell time. Indentations with large enough loads produced median cracks around the indentation. The lengths of these cracks permit estimation of the fracture toughness of the materials by means of the expression [26]:

$$K_{IC} = 0.024(c / a)^{-3/2} \cdot H_v \cdot a^{1/2} \quad (2)$$

where c is the trace length of the crack measured from the center of the indentation, a is one half of the average length of the two indent diagonals, and H_v is the hardness.

The Vickers hardness and the fracture toughness of the (W,Ti)C, (W,Ti)C-5 vol.%FeAl, and (W,Ti)C-10 vol.%FeAl samples were 2652, 2367, 2190 kg/mm^2, and 7, 10, 12 MPa $\cdot$ m$^{1/2}$, respectively. These values represent the average of five measurements. A Vickers hardness indentations in the (W,Ti)C, (W,Ti)C-5 vol.%FeAl, and (W,Ti)C-10 vol.%FeAl samples are shown in Fig. 6, which shows typically, one to three additional cracks were observed to propagate radially from the indentation. It is seen that addition of FeAl to (W,Ti)C significantly improves the fracture toughness of cemented (W,Ti)C without greatly decreasing the hardness. The sintering method in this study was proven to be very effective to consolidate (W,Ti)C-FeAl cermets. Also comparing this investigation of (W,Ti)C-5 vol.%FeAl, and (W,Ti)C-10 vol.%FeAl with a study of WC-10Co and WC-10Ni [27], there is a little difference in fracture toughness but hardness in this study is higher than that in the other study [27] due to high hardness of FeAl.

The hardness of metal carbide greatly decreased by

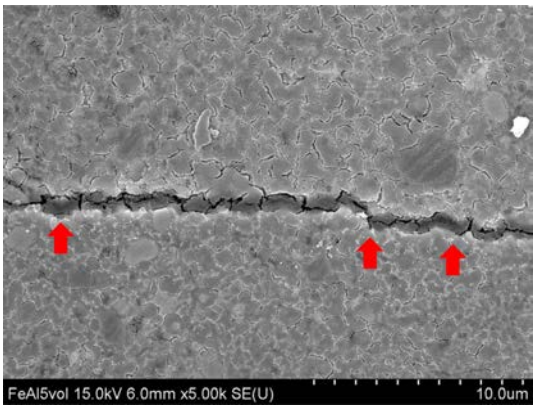

Fig. 7. Crack propagation in (W,Ti)C-10 vol.%FeAl hard materials produced by PCAS.

addition of Co or Ni [27]. The use of FeAl binder instead of Co or Ni is very effective especially to maintain the high hardness of monolithic (W,Ti)C without the expense of toughness reduction. In this regard, it would be worthwhile to consider FeAl as the possible replacement for Co or Ni especially for the applications requiring a high hardness. Kang et al. [28] fabricated (W,Ti)C from nanopowder at 1510 ºC for 1 h by conventional sintering. The grain size of (W,Ti)C was 1-2 μm and hardness and fracture toughness of the (W,Ti)C were 18.9 GPa and 7.2 MPa · $m^{1/2}$, respectively. In our study, nearly full density of (W,Ti)C was obtained at lower temperature and within shorter time. The fracture toughness of (W,Ti)C was similar but hardness of (W,Ti)C was very higher due to refinement of grain size in our study.

Fig. 7 shows a crack propagated in a deflective manner (↑) in (W,Ti)C-10 vol.%FeAl composite. The enhanced fracture toughness of (W,Ti)C-10 vol.%FeAl composite is believed that (W,Ti)C and FeAl in the composite may deter the propagation of cracks and (W,Ti)C and FeAl have nanostructure phases.

Conclusions

Using pulsed current activated sintering (PCAS), the rapid consolidation of the (W,Ti)C, (W,Ti)C-5 vol.%FeAl, and (W,Ti)C-10 vol.%FeAl hard materials was accomplished. Nearly fully dense (W,Ti)C and (W,Ti)C-FeAl composites could be obtained within 3 minutes. The densification temperature of (W,Ti)C was reduced remarkably by the addition of FeAl. The grain size of (W,Ti)C in (W,Ti)C, (W,Ti)C-5 vol.%FeAl, and (W,Ti)C-10 vol.%FeAl hard materials were about 60, 62, and 71 nm, respectively. The Vickers hardness and the fracture toughness of the (W,Ti)C, (W,Ti)C-5 vol.%FeAl, and (W,Ti)C-10 vol.%FeAl samples were 2652, 2367, 2190 kg/mm^2, and 7, 10, 12 MPa · $m^{1/2}$, respectively. The addition of FeAl to (W,Ti)C improved the fracture toughness of cemented (W,Ti)C without great reduction of hardness. The hardness of metal carbide greatly decreased by addition of Co or Ni. The use of FeAl binder instead of Co or Ni is very effective especially to maintain the high hardness of monolithic (W,Ti)C without the expense of toughness reduction. In this regard, it would be worthwhile to consider FeAl as the possible replacement for Co or Ni especially for the applications requiring a high hardness. The hardness of (W,Ti)C consolidated by PCAS was very higher than that of (W,Ti)C sintered by conventional method due to refinement of grain size.

Acknowledgments

This work was supported by a grant in aid awarded by the Basic Research Project of the Korea Institute of Geoscience and Mineral Resources (KIGAM), funded by the Ministry of Science, ICT and Future Planning (GP2015036) and this research was supported by Basic Science Research Program though the National Research Foundation of Korea (NRF) funded by the Ministry of Education (2015R1D1A1A01056600) and this work was supported by the Korea Institute of Energy Technology Evaluation and Planning(KETEP) and the Ministry of Trade, Industry & Energy(MOTIE) of the Republic of Korea (No. 20164030201070).

References

1. S. Imasato, K. Tokumoto, T. Kitada, S. Sakaguchi, Int. J. Refract. Met. Hard Mater. 13 (1995) 305-312.
2. E.A. Almond, B. Roebuck, Mater. Sci. Eng. A 105-106 (1988) 237-248.
3. G. Gille, J. Bredthauer, B. Gries, B. Mende, Int. J. Refract. Met. Hard Mater. 18 (2000) 87-102.
4. P. Goeuriot, F. Thevenot, Ceramics International 13 (1987) 99-103.
5. Z.G. Zhang, F. Gesmundo, P.Y. Hou, Y. Niu, Corrosion Science 48 (2006) 741-765.
6. H. Gleiter, Progress in Materials Science 33 (1989) 223-315.
7. G.E. Fougere, J.R. Weertman, R.W. Siegel, S. Kim, Scripta Metallurgica et Materialia 26 (1992) 1879-1883.
8. I.J. Shon, H.J. Kwon, H.S. Oh, Electron. Mater. Lett. 10 (2014) 337-343.
9. H.S. Kang, J.M. Doh, J.K. Yoon, I.J. Shon, Korean J. Met. Mater. 52 (2014) 759-764.
10. F. Charlot, E. Gaffet, B. Zeghmati, F. Bernard, J.C. Liepce, Mater. Sci. Eng. A 262 (1999) 279-278.
11. H.S. Kang, I.J. Shon, Korean J. Met. Mater. 52 (2014) 623-629.
12. M.K. Beyer, H. Clausen-Schaumann, Chem. Rev. 105 (2005) 2921-2948.
13. Bong-Won Kwak, Byung-Su Kim, Jin-Kook Yoon, Kyung-Tae Hong and In-Jin Shon, Journal of Ceramic Processing Research. Vol. 16, No. 3 (2015) 340-345.
14. I.J. Shon, Korean J. Met. Mater. 52 (2014) 573-580.
15. I.J. Shon, H.G. Jo, B.S. Kim, J.K. Yoon, K.T. Hong, Korean J. Met. Mater. 53 (2015) 474-479.
16. I.J. Shon, H.G. Jo, H.J. Kwon, Korean J. Met. Mater. 52 (2014) 343-346.
17. C. Suryanarayana, M. Grant Norton, X-ray Diffraction A

Practical Approach, Plenum Press, New York, 1998.
18. S.M. Kwon, N.R. Park, J.W. Shin, S.H. Oh, B.S. Kim, I.J. Shon, Korean J. Met. Mater. 53 (2015) 555-562.
19. B.R. Kang, J.K. Yoon, K.T. Hong, I.J. Shon, Met. Mater. Int. 21 (2015) 698-703.
20. B.R. Kang and I.J. Shon, Korean J. Met. Mater. 53 (2015) 320-325.
21. G.S. Upadhyaya, Materials & Design 22 (2001) 483-489.
22. Z. Shen, M. Johnsson, Z. Zhao, M. Nygren, J. Am. Ceram. Soc. 85 (2002) 1921-1927.
23. J.E. Garay, U. Anselmi-Tamburini, Z.A. Munir, S.C. Glade, P. Asoka-Kumar, Appl. Phys. Lett. 85 (2004) 573-575.
24. J.R. Friedman, J.E. Garay, U. Anselmi-Tamburini, Z.A. Munir, Intermetallics 12 (2004) 589-597.
25. J.E. Garay, U. Anselmi-Tamburini, Z.A. Munir, Acta. Mater. 51 (2003) 4487-4495.
26. K. Niihara, R. Morena, D.P.H. Hasselman, J. Mater. Sci. Lett. 1 (1982) 12-16.
27. I.J. Shon, I.K. Jeong, I.Y. Ko, J.M. Doh, K.D. Woo, Ceramics International 35 (2009) 339-344.
28. J. Jung, S. Kang, Scripta Materialia 56 (2007) 561-564.